depicting the multiple functions of IPMK as a soluble InsPs kinase, and as a PI3-kinase acting on both membrane bound PIP_2 and SF-1/PIP_2. SF-1 transcriptional output is affected after IPMK and PTEN modify the solvent-exposed phospholipid head group present in the bound PIP_2 or PIP_3 ligands.

Fig. S1. p110γ, the kinase dead rIPMK mutant (D127A), and IP_3 kinase fail to generate PIP_3 from SF-1/PIP_2. HPLC chromatographs of glyceroinositol head groups after ^{32}P-γATP IVK reactions using 100nM (**A**) WT rIPMK, (**B**) KD rIPMK, (**C**) human p110α/p85α or (**D**) p110γ, incubated with either PIP_2/PS micelles (left panels) or 1 μM SF-1/PIP_2 substrate (right panels), as indicated, for 30 min at 37C. Migration of glyceroinositol (1,3,4,5)P following deacylation of PIP_3 is indicated with red arrowheads. **E**) Autoradiography of 10 minute IVK reactions on 10 μM SF-1/PIP_2 analyzed by nitrocellulose capture, using indicated concentrations of indicated enzymes.

Fig. S2. Enzyme/Substrate Kinetic Parameters, and Ins(1,4,5)P competitive inhibition of IPMK activity on SF-1/PIP_2. Human IPMK velocities plotted against increasing substrate concentrations as measured by nitrocellulose capture assays of IVK reactions. Data were fit to (**A**) linear double-reciprocal (Lineweaver-Burke) and non-linear (Michaelis-Menton, Refer to Fig. 2) curves by GraphPad Prism software. (**B**) Non-linear and linear curve fits of IPMK reaction velocities on SF-1/PIP_2 as determined above, except in the presence of indicated [Ins(1,4,5)P]. Data are presented fitted to non-linear and linear plots, fitted as in (A). (**C**) Table of kinetic parameters at each Ins(1,4,5)P

concentration shows a constant V_{MAX}, with a changing K_M; values are expressed in the bar graph (right). **(D)** PTEN activity on SF-1/PIP_2 was measured by extracting the PTEN reaction product (SF-1/PIP_2) into 1:1 MeOH:$CHCl_3$ and coupling to a p110α/p85α ^{32}P-γATP IVK reaction, as described in materials and methods. Data were fit to non-linear Michaelis-Menton and linear double-reciprocal Lineweaver-Burke curves by GraphPad Prism software.

Fig. S3 Overexpression of different IPMKs has no effect on SF-1 transcripts. (**A**) *SF-1* transcripts after siIPMK or siCON followed by transient transfection of indicated IPMK expression constructs, as described in Methods. (**B**) Expression of myc-tagged IPMK proteins in HEK 293 SF-1 cells treated identically as in (A).

Fig. S4. SF-1 transcripts and nuclear localization are unaffected by ATA. Wortmannin does not recapitulate ATA effects on SF-1 target genes (**A**) SF-1 transcript levels are shown in WT and Pocket Mutant (A270W, L345F) HEK 293 SF-1 cells following ATA or EGCG treatment. (**B**) Immunocytochemistry of 3X-FLAG tagged SF-1 in HEK 293 SF-1 cells treated with vehicle or ATA, as described in Materials and Methods. (**C**) IPMK activity on SF-1/PIP_2 in the presence of indicated compounds at indicated concentrations. (**D**) qPCR measuring transcript levels of indicated genes in HEK 293 SF-1 cells after 14 hrs treatment with wortmannin (WORT, 10 μM) or DMSO vehicle control.

Fig S5. The SF-1 protein component purified from HEK 293 cells is not phosphorylated by recombinant IPMK. (**A**) Silver stained SDS-PAGE of FLAG-peptide eluates from TET-induced HEK 293 SF-1 cells demonstrating purity of SF-1 protein. Molecular weight standards are indicated to the left. Western blot of FLAG peptide eluates from EtOH and TET-induced HEK 293 SF-1 cells probed with anti-FLAG antibodies. (**B**) Autoradiography of IVK reactions (shown in Figure 6A) separated by SDS-PAGE (upper panel). Following exposure for 18 hrs, gels were silver stained to confirm equal loading of lanes and the presence of all SF-1 and IPMK proteins; experimental conditions in each reaction are indicated.

Table S1 RT-qPCR Primers

Gene	Accession	Forward Primer Sequence	Reverse Primer Sequence
mSF-1 (NR5A1)	NM_139051	CGTCTGTCTCAAGTTCCTCATCCT	TCCTTTACGAGGCTGTGGTTGT
hSHP (NR0B2)	NM_021969	GCTTAGCCCCAAGGAATATGC	TTGGAGGCCTGGCACATC
hStAR	NM_000349	CCCATGGAGAGGCTCTATGAA	GTTCCACTCCCCCATTGCT
hCYP17A1	NM_000102	AGGACTTCTCTGGGCGGCCT	GTGTGCGCCAGAGTCAGCGA
hCYP11A1	NM_000781	GGGTCGCCTATCACCAGTATT	GCTGCCGACTTCTTCAACAG
hGAPDH	NM_002046	CAAGGTCATCCATGACAACTTTG	GGCCATCCACAGTCTTCTGG
hTBP	NM_003194	CCTAAAGACCATTGCACTTCGT	AGCAAACCGCTTGGGATTA

Table S2 ChIP-qPCR Primers

Gene	Accession	Forward primer sequence	Reverse primer sequence
hHSP70	NM_198431	TCTGGAGAGTTCTGAGCAGG	CCCTTCTGAGCCAATCACCG
hStAR	NM_000349	CCACAAACGGCCAAGCA	CGCCATCACTCACTGTGCAA

Fig. S1, Blind, et al.

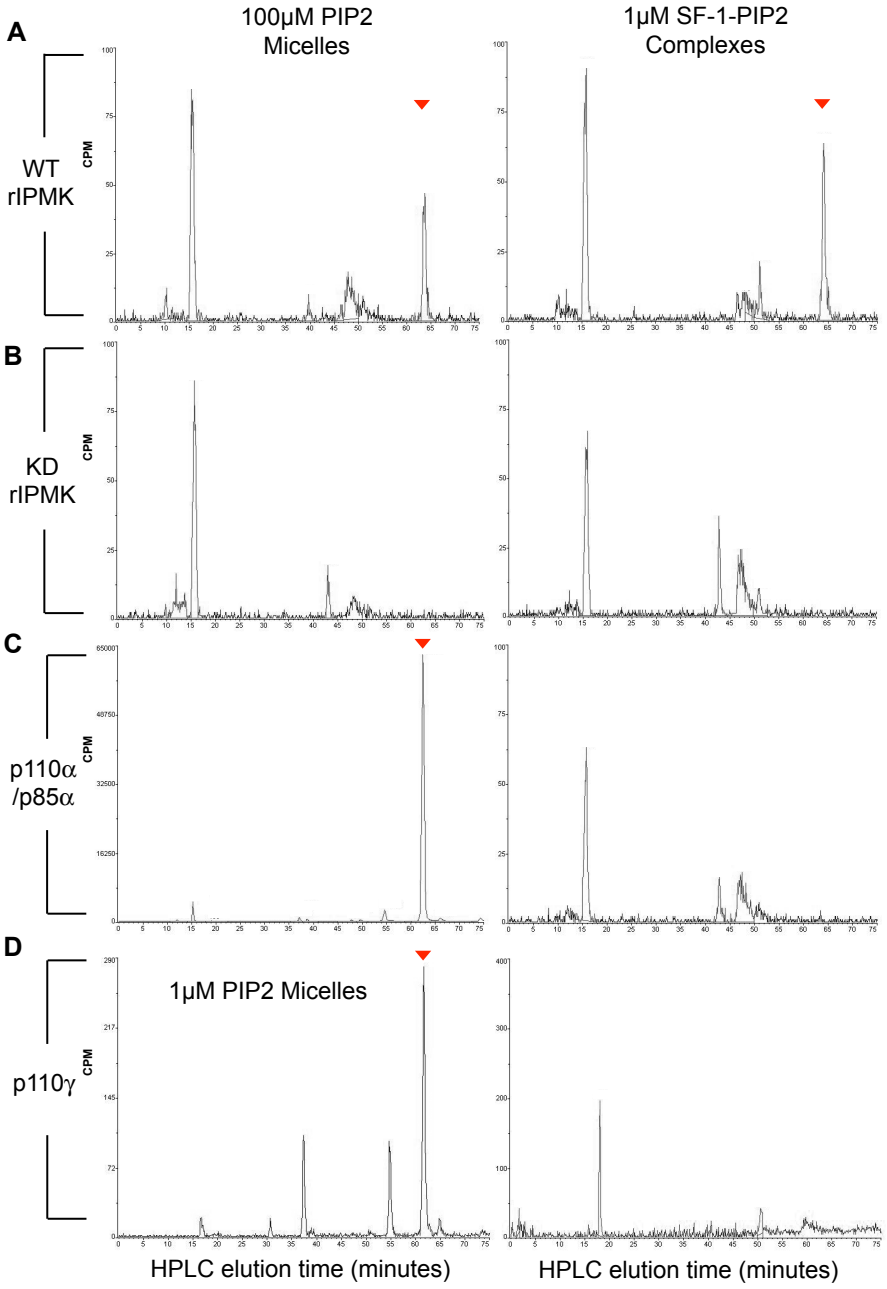

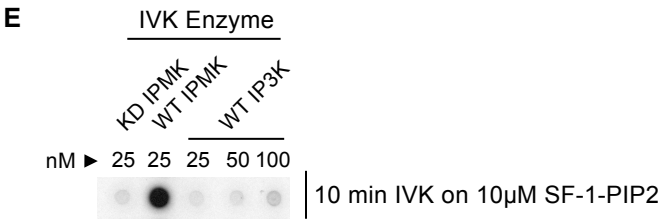

Fig. S2, Blind., et al.

A

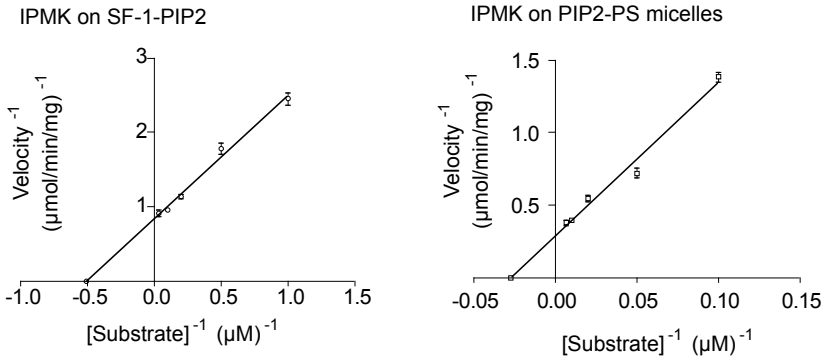

B

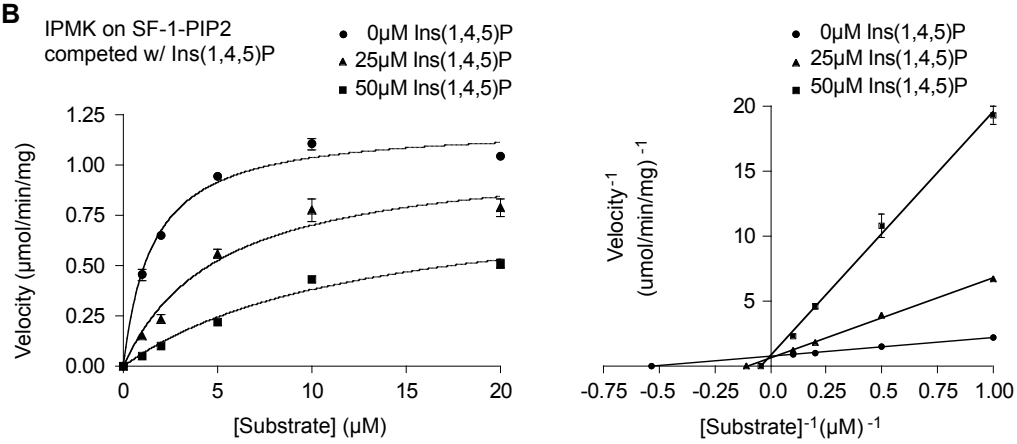

C

IPMK on SF-1-PIP2
competed w/ Ins(1,4,5)P

	0µM	25µM	50µM
curve fit (r^2)	0.999	0.998	0.998
KM (*µM*)	**1.87**	**9.29**	**23.27**
VMAX (*µmol/min/mg*)	**1.29**	**1.51**	**1.24**
kcat (s^{-1})	1.11	1.29	1.07
kcat/KM ($s^{-1} M^{-1}$)	593,263	139,785	45,827

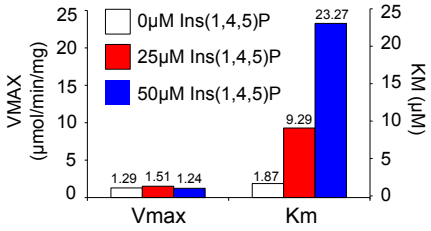

D

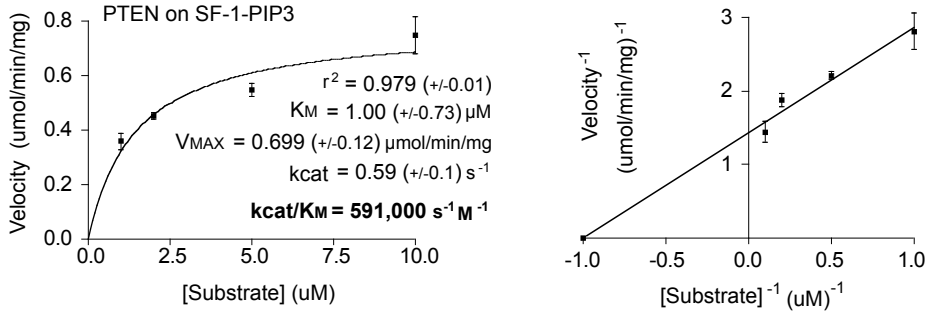

Fig. S3. Blind, et al.

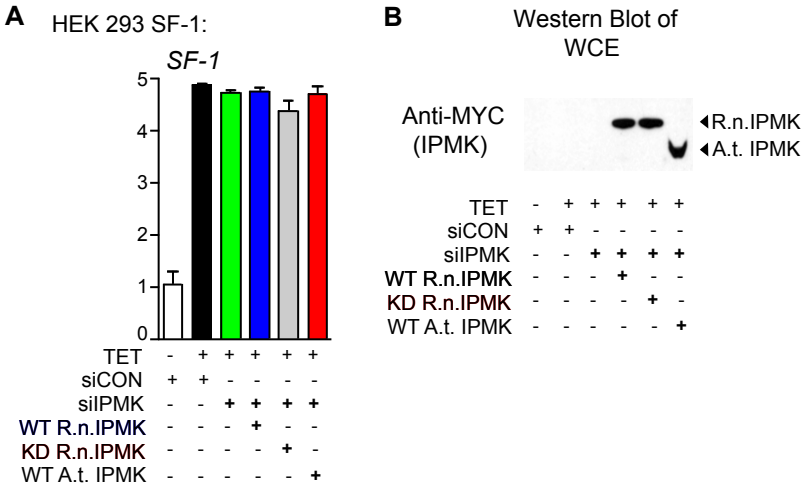

Fig. S4. Blind, et al.

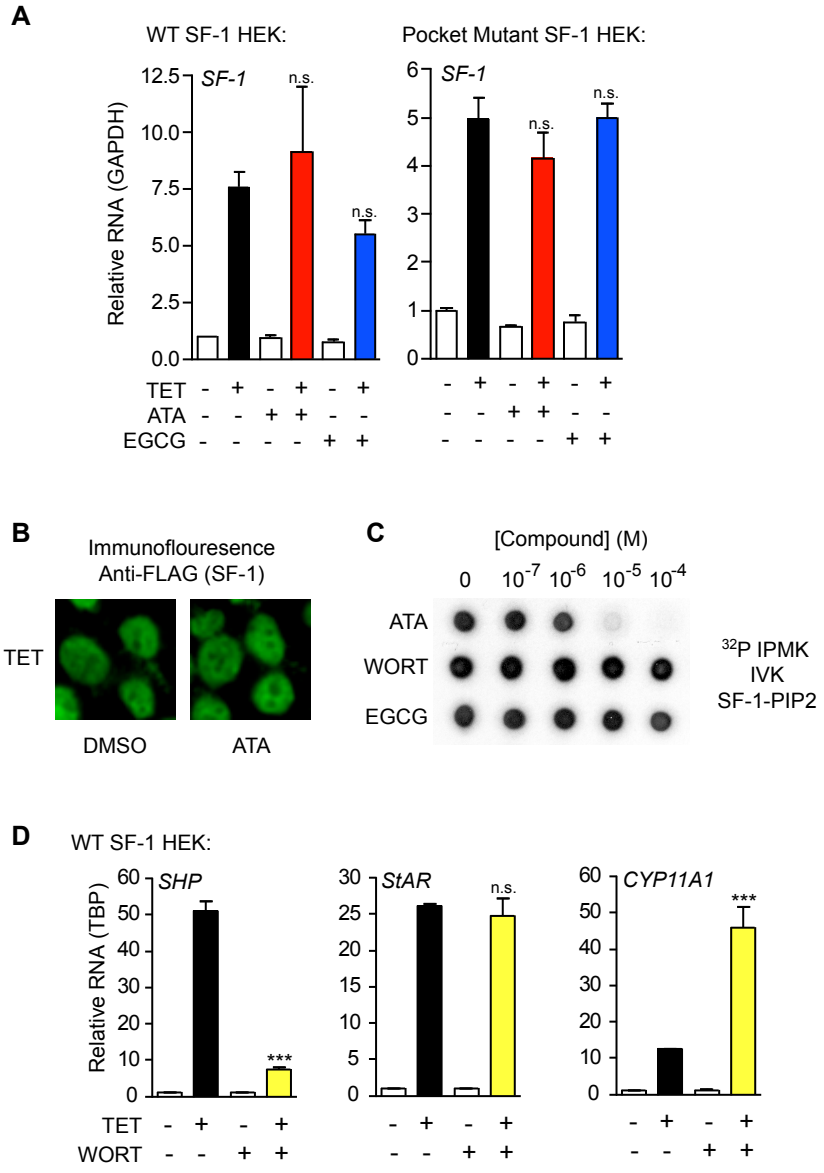

Fig. S5, Blind., et al.